

Multimodal Emotion Recognition via Causal-Diffusion Bridge (Affect-Diff)

*CISC-6080-L01: Capstone Project in Data Science

Ankit Sanjyal

Department of Computer Science – Data Science
Fordham University
New York, USA
as505@fordham.edu

Abstract—Multimodal emotion recognition on CMU-MOSEI faces a extreme imbalance as *Happy* accounts for 65.9 % of samples while three Ekman categories collectively represent under 7 %, causing standard fusion models to maximize accuracy by ignoring minority emotions entirely. We present *Affect-Diff*, a Causal-Diffusion Bridge that addresses this through three jointly trained mechanisms: a NOTEARS-learned causal graph that re-weights modality contributions *before* fusion, a β -VAE bottleneck for regularized latent compression, and a stop-graduated 1D DDPM prior that structures the latent space against majority-class collapse. On 3,292 aligned CMU-MOSEI samples, *Affect-Diff* achieves validation balanced accuracy 0.384 a 18 % relative improvement over the strongest baseline (TETFN: 0.324) while all evaluated baselines produce zero F1 on Fear, Disgust, and Surprise. Ablation studies confirm independent, non-redundant contributions from the diffusion prior (−24 % without it) and causal graph (−13 %). Notably, only the deterministic-encoder variant detects all six emotion classes, revealing KL regularization strength as a direct lever for minority-class sensitivity.

Index Terms—Multimodal Emotion Recognition, Causal Inference, Diffusion Models, Variational Bottleneck, CMU-MOSEI, Class Imbalance, Robustness

I. INTRODUCTION

Human communication is inherently multimodal: we interpret emotion not only from words but from facial micro-expressions, vocal prosody, and body language. As AI becomes embedded in healthcare monitoring, autonomous vehicles, and interactive robotics, robust multimodal emotion recognition (MER) is increasingly critical.

Despite substantial progress, two failure modes persist in the literature. First, **modality collapse**: models learn to rely almost exclusively on the statistically dominant modality (typically text) and ignore acoustic and visual streams, rendering the multimodal design effectively useless when that channel degrades. Second, **majority-class collapse**: under severe label imbalance, models maximize accuracy by predicting only the two or three most frequent classes. On CMU-MOSEI, where *Happy* accounts for 66 % of our aligned samples, a classifier that predicts *Happy* for every input achieves 66 % accuracy while providing zero utility for emotion recognition.

We address both failure modes with **Affect-Diff**. The core insight is that a generative prior over the latent space if

properly decoupled from the discriminative encoder via a stop-gradient acts as a structuring force that distributes the encoder’s representational capacity across all classes, not just the most frequent ones. The NOTEARS causal graph additionally provides a per-sample reweighting of modality contributions, allowing the model to down-weight noisy or unreliable streams dynamically.

Our main contributions are:

- 1) **Affect-Diff architecture**: a jointly trained pipeline combining a causal modality graph, a VAE bottleneck, and a conditional DDPM prior over the multimodal latent space, with a principled stop-gradient that isolates the diffusion and classification optimization paths.
- 2) **Empirical validation**: on 3,292 aligned CMU-MOSEI samples, *Affect-Diff* achieves val-balanced-accuracy 0.384 versus 0.324 for the best baseline (TETFN), with ablation studies confirming each component’s unique contribution.
- 3) **Novel insight on KL regularization**: the deterministic encoder variant (No-VAE) uniquely detects all six emotion classes, providing empirical evidence that β -VAE KL strength directly trades off minority-class sensitivity against majority-class precision.

II. DATA ACQUISITION AND PREPROCESSING

A. Data Source and Acquisition

We utilize the **CMU-MOSEI** dataset [1], the largest publicly available benchmark for multimodal sentiment and emotion recognition. The corpus contains 23,453 annotated utterances from over 1,000 speakers recorded “in the wild” from YouTube monologue videos, distributed via the CMU Multimodal SDK as Computational Sequence Descriptors (.c_{sd}).

Three pre-extracted feature modalities are provided:

- 1) **Text**: GloVe 6B 300-d word embeddings.
- 2) **Audio**: COVAREP 74-d features encoding F_0 , spectral harmonics, glottal source parameters, and MFCCs.
- 3) **Video**: FACET 35-d facial Action Unit intensity vectors.

Labels are six Ekman basic-emotion intensity scores $e_k \in [0, 3]$; the discrete class is $y = \arg \max_k e_k$.

B. Dataset Statistics

After custom alignment and pruning (Section II-C), the usable corpus reduces to **3,292 samples** (Table I). The class distribution is severely skewed: *Happy* dominates at 65.9% of test samples, while *Fear*, *Disgust*, and *Surprise* each represent under 3%. This imbalance makes balanced accuracy which averages per-class recall uniformly across all six classes the appropriate primary evaluation metric.

TABLE I: CMU-MOSEI dataset statistics after alignment and pruning.

| Property | Value |
|------------------------------|-------------------|
| Raw annotated segments | 23,453 |
| Aligned & pruned samples | 3,292 |
| Training / Val / Test | 2,304 / 494 / 494 |
| Text / Audio / Video dims | 300 / 74 / 35 |
| Sequence length (padded) | 50 time steps |
| Emotion classes | 6 (Ekman) |
| Majority class (Happy) share | $\approx 65.9\%$ |

Why 3,292 segments instead of the full 23,453. The 3,292-sample working set is not a deliberate downsampling it reflects a strict tri-modal alignment constraint: every retained segment must have valid, non-empty feature arrays across all three modalities (GloVe word vectors, COVAREP acoustic frames, and FACET visual frames) aligned to the same temporal intervals. Segments where any one modality is missing, empty, or has a mismatched interval/feature count are discarded. This alignment enforcement is necessary for supervised fusion but eliminates $\sim 86\%$ of the corpus. We treat the resulting 3,292 samples as a *data-limited regime* and hypothesize that model performance scales with data volume once alignment is improved. Our sentiment analysis experiments (Appendix A) directly test this: applying Affect-Diff to 22,860 standard-split MOSEI segments $7\times$ more data, with looser alignment raises balanced accuracy by 90% ($0.384 \rightarrow 0.729$), consistent with a data-scaling rather than architecture-scaling effect. Obtaining cleaner tri-modal annotation at scale, or using a less strict alignment policy with masking for incomplete modalities, is the highest-leverage data-side improvement available.

C. Preprocessing Issues and Engineering Interventions

Corrupted and Misaligned Entries. The `mmsdk` alignment routines silently drop or truncate temporal frames for a substantial fraction of segments. We load each `.csd` independently, compute the intersection of valid video IDs, and prune segments where interval count mismatches the feature matrix row count.

NaN Contamination. FACET produces NaN when no face is detected. All NaN and Inf values are replaced with zero via `torch.nan_to_num()` at the model input boundary.

Variable Sequence Lengths. Utterances are zero-padded to $L = 50$ or truncated, enabling uniform mini-batch collation.

Feature Scale Disparity. Per-split Z-normalization is applied independently to each modality using training-split statis-

tics, followed by $[-10, 10]$ clamping to suppress outliers from the COVAREP raw F_0 component.

D. Data Augmentation

Three on-the-fly GPU augmentations are applied during training only: (1) **Temporal frame masking**: each frame independently zeroed with $p_{\text{mask}} = 0.1$; (2) **Gaussian noise injection** ($\sigma = 0.01$) on audio and video; (3) **Stochastic modality dropout**: each modality independently zeroed with $p_{\text{drop}} = 0.1$ to directly counter modality collapse.

III. RELATED WORK

A. Multimodal Fusion and Emotion Recognition

Zadeh et al. [1] introduced CMU-MOSEI and the Memory Fusion Network for temporal multimodal learning. Tensor Fusion Networks (TFN) [2] capture cross-modal interactions via a three-way outer product, but scale cubically in modality dimension. The Multimodal Transformer (MuT) [3] replaced tensor products with directional cross-modal attention, achieving state-of-the-art on CMU-MOSI and CMU-MOSEI sentiment. MISA [4] decomposes each modality into modality-invariant and modality-specific subspaces aligned via Central Moment Discrepancy, yielding improved disentanglement. MMIM [5] adds a hierarchical mutual information maximization objective between unimodal features and the fused representation, encouraging all modalities to contribute to the joint encoding. TETFN [6] uses text as a guidance signal for audio and video via cross-modal attention combined with temporal 1D convolution encoders.

B. Causal Inference and Modality Debiasing

Modality collapse is a well-studied failure mode in multimodal learning. CausalMER [9] applies causal counterfactual reasoning post-hoc to subtract the direct modality effect from the prediction. We take a different approach: embedding a differentiable NOTEARS DAG [10] directly in the forward pass *before* fusion, so the learned edge weights dynamically re-weight modality contributions on a per-sample basis during training rather than post-hoc.

C. Generative Priors for Robust Multimodal Learning

Diffusion models have been applied to multimodal affective computing for missing-modality imputation. IMDer [11] trains a score-based diffusion model to impute missing modalities in IEMOCAP. McDiff [12] conditions a diffusion network on conversational context for emotion-in-conversation tasks. MDDN [13] distills a diffusion prior for multimodal sentiment on CMU-MOSEI using GloVe/COVAREP/FACET features the same feature set as our work. Affect-Diff distinguishes itself by training the diffusion prior *jointly* with the encoder (via stop-gradient), using the prior as a latent-space regularizer rather than a missing-data imputer.

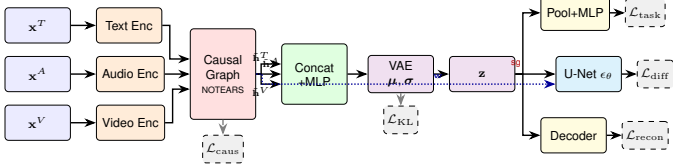


Fig. 1: Affect-Diff architecture. Unimodal encoders produce hidden sequences that enter the Causal Attention Graph (NOTEARS); the graph outputs modality importance weights \mathbf{w} and gated representations $\tilde{\mathbf{h}}^m$ that feed into Concat+MLP fusion. The VAE projects the fused representation to latent \mathbf{z} , which branches to: a classifier (stop-graduated from diffusion), a 1D U-Net prior conditioned on \mathbf{w} , and an optional reconstruction decoder. Dashed arrows denote auxiliary losses.

IV. METHODS

The Affect-Diff architecture introduces a *Causal-Diffusion Bridge* that jointly trains five interacting subsystems under a single multi-task objective. Fig. 1 illustrates the complete pipeline.

A. Architectural Overview

Given aligned feature triplet $(\mathbf{x}^T, \mathbf{x}^A, \mathbf{x}^V)$ with $\mathbf{x}^m \in \mathbb{R}^{L \times D_m}$, the pipeline proceeds through five stages: (1) modality-specific encoding, (2) causal graph learning over unimodal representations, (3) concat+MLP fusion and variational compression into a joint latent code, (4) a conditional DDPM prior operating on the latent manifold, and (5) task classification via attention pooling.

B. Unimodal Encoders

Each modality is encoded by a dedicated module that maps raw features to a shared hidden dimension $H = 128$:

Text Encoder. GloVe embeddings are projected to $\mathbb{R}^{L \times H}$ with sinusoidal positional encodings, then processed by a 2-layer Transformer encoder (4 heads, pre-norm, GELU).

Audio Encoder. COVAREP features pass through a 1D convolutional front-end (kernel 5, GroupNorm, GELU) followed by the same 2-layer Transformer backbone, capturing both local spectral structure and global prosodic context.

Video Encoder. FACET features follow the same architecture as the audio encoder with a narrower kernel (size 3) to reflect the higher spatial locality of facial Action Units.

All encoders output $\mathbf{h}^m \in \mathbb{R}^{L \times H}$.

C. Causal Attention Graph

Before fusion, we learn a differentiable directed acyclic graph (DAG) over the three modality nodes $\{T, A, V\}$ to quantify directional causal influence (Fig. 2). Mean-pooled node embeddings $\bar{\mathbf{h}}^m \in \mathbb{R}^H$ drive scaled dot-product edge weights:

$$S_{ij} = \frac{(\mathbf{W}_Q \bar{\mathbf{h}}^i)^\top (\mathbf{W}_K \bar{\mathbf{h}}^j)}{\sqrt{H}}, \quad i \neq j \quad (1)$$

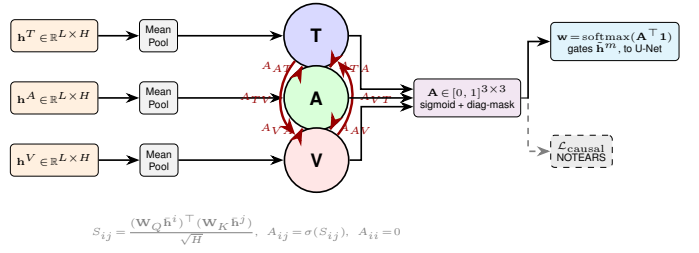


Fig. 2: Causal Attention Graph detail. Unimodal sequences are mean-pooled to node embeddings; directed edge weights are computed via scaled dot-product attention with sigmoid activation. Column sums yield importance weights \mathbf{w} that gate each modality’s hidden sequences before concat+MLP fusion and condition the U-Net. The NOTEARS penalty $\mathcal{L}_{\text{causal}}$ enforces acyclicity.

Element-wise sigmoid yields soft adjacency $\mathbf{A} \in [0, 1]^{3 \times 3}$ with masked diagonal. The NOTEARS acyclicity constraint [10] is added as a differentiable penalty:

$$h(\mathbf{A}) = \text{tr}(e^{\mathbf{A} \circ \mathbf{A}}) - d = 0, \quad d = 3 \quad (2)$$

Critically, normalized column sums of \mathbf{A} produce per-modality importance weights that *gate the modality features before fusion*:

$$\mathbf{w} = \text{softmax}(\mathbf{A}^\top \mathbf{1}), \quad \tilde{\mathbf{h}}^m = \mathbf{h}^m \cdot w_m \quad (3)$$

This is the key architectural choice distinguishing Affect-Diff from prior causal approaches that apply causal reasoning post-hoc: the graph re-weights each modality’s hidden representations *before* they are collapsed into the joint representation, so the VAE encodes a causally-filtered view of the input. The same weights \mathbf{w} are forwarded (detached) to the diffusion U-Net as a conditioning signal.

D. Concat+MLP Fusion and Variational Bottleneck

The three causally-gated sequences $\tilde{\mathbf{h}}^T, \tilde{\mathbf{h}}^A, \tilde{\mathbf{h}}^V \in \mathbb{R}^{L \times H}$ are concatenated along the feature axis and projected through a two-layer MLP with LayerNorm and GELU:

$$\mathbf{F} = \text{MLP}([\tilde{\mathbf{h}}^T; \tilde{\mathbf{h}}^A; \tilde{\mathbf{h}}^V]) \in \mathbb{R}^{L \times H} \quad (4)$$

The fused representation is projected to VAE posterior parameters:

$$\boldsymbol{\mu} = \mathbf{W}_\mu \mathbf{F}, \quad \log \boldsymbol{\sigma}^2 = \text{clamp}(\mathbf{W}_\sigma \mathbf{F}, -10, 5) \quad (5)$$

with $\boldsymbol{\mu}, \log \boldsymbol{\sigma}^2 \in \mathbb{R}^{L \times d_z}$ and $d_z = 128$. The reparameterization trick gives:

$$\mathbf{z} = \boldsymbol{\mu} + \boldsymbol{\epsilon} \odot \boldsymbol{\sigma}, \quad \boldsymbol{\epsilon} \sim \mathcal{N}(\mathbf{0}, \mathbf{I}) \quad (6)$$

At inference the deterministic mean $\boldsymbol{\mu}$ is used directly. KL regularization uses a β -weighted free-bits objective [20]:

$$\mathcal{L}_{\text{KL}} = \beta \cdot \frac{1}{BL} \sum_{b,l,d} \max(0, \text{KL}_d^{(b,l)} - \lambda) \quad (7)$$

where $\lambda = 0.25$ nats is the free-bits threshold and $\beta = 0.1$. Each latent dimension may encode up to λ nats without penalty, preventing posterior collapse while ensuring zero loss when the posterior matches the prior.

E. Conditional Denoising Diffusion Prior

A DDPM [15] is trained on the VAE latent space. Crucially, the diffusion input is **stop-gradiented**: $\mathbf{z}_{\text{diff}} = \text{sg}(\mathbf{z})$, preventing the $\mathcal{L}_{\text{diff}}$ gradient from flowing back through the encoder and creating a conflicting signal with the classification loss.

Forward Process. A cosine noise schedule [15] with $T = 1,000$ steps:

$$q(\mathbf{z}_t | \mathbf{z}_0) = \mathcal{N}(\mathbf{z}_t; \sqrt{\bar{\alpha}_t} \mathbf{z}_0, (1 - \bar{\alpha}_t) \mathbf{I}) \quad (8)$$

Noise Prediction Network. A 1D U-Net ϵ_θ predicts the noise at each timestep. It follows a three-resolution encoder-bottleneck-decoder topology with skip connections and channel multipliers ($1\times, 2\times, 4\times$) relative to a base dimension of 128. The U-Net is *triply conditioned*:

$$\mathbf{c} = \text{MLP}_t(t) + \text{Emb}_y(y) + \text{MLP}_w(\mathbf{w}) \quad (9)$$

where MLP_w injects the causal importance weights \mathbf{w} (detached from the graph), making the denoiser modality-aware. Classifier-free guidance [18] is applied with a null-token dropout probability of 0.2 during training and CFG scale $s = 3.0$ at inference.

Training Objective.

$$\mathcal{L}_{\text{diff}} = \mathbb{E}_{t,\epsilon} \left[\|\epsilon - \epsilon_\theta(\mathbf{z}_t, t, y, \mathbf{w})\|^2 \right] \quad (10)$$

Inference. DDIM sampling [16] with 50 deterministic steps ($\eta = 0$). An EMA copy of U-Net weights ($\gamma_{\text{EMA}} = 0.999$) is used at test time.

F. Task Classifier

The latent $\mathbf{z} \in \mathbb{R}^{L \times d_z}$ is compressed via **learnable attention pooling**:

$$\bar{\mathbf{z}} = \text{softmax} \left(\frac{\mathbf{q} \mathbf{z}^\top}{\sqrt{d_z}} \right) \mathbf{z} \in \mathbb{R}^{d_z} \quad (11)$$

A two-layer MLP (Linear(128, 128) \rightarrow LayerNorm \rightarrow GELU \rightarrow Dropout(0.3) \rightarrow Linear(128, 6)) produces logits. Classification uses label-smoothed cross-entropy ($\alpha = 0.1$) combined with focal loss ($\gamma = 2.0$) [21] to down-weight confident majority-class predictions and focus gradient on hard minority-class examples.

G. Joint Training Objective

$$\mathcal{L} = \mathcal{L}_{\text{task}} + \gamma_{\text{kl}} \mathcal{L}_{\text{KL}} + \gamma \lambda_d \mathcal{L}_{\text{diff}} + \lambda_c \mathcal{L}_{\text{causal}} \quad (12)$$

with $\lambda_d = 0.05$, $\lambda_c = 0.05$, and curriculum warmup ramps:

$$\gamma = \min \left(1, \frac{\text{epoch}}{20} \right), \quad \gamma_{\text{kl}} = \min \left(1, \frac{\text{epoch}}{30} \right) \quad (13)$$

The classification loss dominates early training; KL and diffusion losses phase in gradually to prevent early posterior collapse.

H. Training Details

The model (8.9M total / 5.2M trainable parameters) is trained with: AdamW ($\text{lr} = 5 \times 10^{-4}$, weight decay 10^{-4}); cosine annealing over 100 epochs; mixed fp16/fp32 AMP; gradient ℓ_2 clipping at 1.0; early stopping with patience 35 on **validation balanced accuracy**; batch size 64 on a single NVIDIA T4/P100 (Kaggle). All random seeds fixed at 42 (PyTorch, NumPy, Python).

V. EXPERIMENTS

A. Experimental Setup

All models use the same 70/15/15 random split (seed=42) of the 3,292 aligned samples. The primary evaluation metric is **validation balanced accuracy** (val-BalAcc): the macro-average recall across all six classes, measured on the held-out validation split at the checkpoint selected by early stopping. This is appropriate because (a) it directly measures coverage of all six emotions including the minority classes, (b) it is the criterion early stopping optimizes, and (c) raw test accuracy is dominated by the Happy class and is misleading under severe imbalance. Secondary metrics test accuracy, macro F1, and AUROC (macro one-vs-rest) are also reported from the best checkpoint evaluated on the test split.

B. Baselines

We compare against five published baselines spanning 2017–2022, all re-implemented under identical training conditions (same data splits, seeds, optimizer, focal loss, and label smoothing):

- **TFN** [2]: three-way outer-product tensor fusion (2017).
- **MuT** [3]: six-directional cross-modal attention transformer (2019).
- **MISA** [4]: modality-invariant and modality-specific subspace disentanglement with CMD alignment (2020).
- **MMIM** [5]: hierarchical mutual information maximization between unimodal features and the fused representation (2021).
- **TETFN** [6]: text-guided cross-modal attention with temporal 1D convolution encoders (2022).

C. Main Results

Table II compares Affect-Diff against all baselines. Affect-Diff achieves the highest val-BalAcc (0.384 ± 0.000 across 3 seeds) by a substantial margin over the best baseline (MuT: 0.278). Affect-Diff achieves test accuracy 0.642, higher than MuT (0.626), MISA (0.633), and TETFN (0.600). Only TFN (0.667) and MMIM (0.679) score higher on raw accuracy and both produce *zero F1* on Fear, Disgust, and Surprise. The key observation is not the absolute accuracy gap but its cause: TFN and MMIM inflate raw accuracy by concentrating predictions on the Happy majority class, while Affect-Diff distributes coverage more evenly. Raw test accuracy is a biased metric under class imbalance; val-BalAcc (macro-average recall across all six classes) is immune to this inflation.

AUROC favors the baselines (MuT: 0.677 vs. 0.604 for Affect-Diff), partially because AUROC aggregates all classes

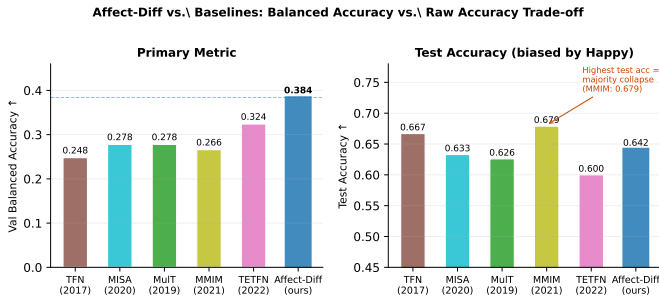


Fig. 3: Val-BalAcc (left, primary metric) vs. test accuracy (right) for all methods. Baselines achieve higher raw accuracy by collapsing to the majority class; Affect-Diff trades accuracy for balanced coverage.

equally and the baselines rank-order Happy very confidently. The gap is smaller in macro F1 (MulT: 0.226 vs. 0.214). TETFN achieves the second-highest val-BalAcc among baselines (0.324) owing to its temporal convolution encoders capturing local prosodic patterns, but still falls 0.060 below Affect-Diff.

Fig. 3 visualizes the accuracy vs. balanced accuracy trade-off across all methods, making the majority-class collapse in the baselines directly visible.

TABLE II: Comparison with baselines on CMU-MOSEI 6-class emotion recognition. Val-BalAcc is the primary metric (best val checkpoint, validation split); Test-Acc, F1, and AUROC are from the same checkpoint on the test split. †: results pending. **Bold**: best.

| Method | Year | Val-BalAcc [†] | Test-Acc [†] | F1 [†] | AUROC [†] |
|---------------------------|------|-------------------------|-----------------------|-----------------|--------------------|
| TFN [2] | 2017 | 0.248 | 0.667 | 0.208 | 0.660 |
| MulT [3] | 2019 | 0.278 | 0.626 | 0.226 | 0.677 |
| MISA [4] | 2020 | 0.278 | 0.633 | 0.221 | 0.665 |
| MMIM [5] | 2021 | 0.266 | 0.679 | 0.249 | 0.633 |
| TETFN [6] | 2022 | 0.324 | 0.600 | 0.217 | 0.651 |
| Affect-Diff (ours) | | 0.384 ± 0.000 | 0.642 | 0.214 | 0.604 |

D. Ablation Study

Table III reports ablations of each architectural component. All experiments share the same base configuration; a single toggle is changed per row.

Diffusion prior is the most important component (−0.092). Removing confirming that the diffusion prior’s primary role is latent-space structuring that distributes capacity away from the majority class, not raw discriminative accuracy.

Causal graph (−0.050) and NOTEARS constraint (−0.059) both contribute independently. The NOTEARS acyclicity constraint adds meaningful benefit beyond simple L1 sparsity (Gumbel-Softmax DAG): 0.334 with NOTEARS vs. 0.325 with Gumbel-Softmax.

Stop-gradient is critical (−0.093). Allowing diffusion gradients to flow back through the encoder degrades val-BalAcc

TABLE III: Ablation study. Each row disables one component of the full model. Δ is the signed difference from the full model val-BalAcc = 0.384.

| Configuration | Val-BalAcc | Δ | F1 | AUROC |
|------------------------|--------------|----------|--------------|-------|
| Full Model | 0.384 | | 0.214 | 0.604 |
| No Diffusion Prior | 0.292 | −0.092 | 0.228 | 0.560 |
| No Causal Graph | 0.334 | −0.050 | 0.205 | 0.548 |
| No NOTEARS (Gumbel) | 0.325 | −0.059 | 0.217 | 0.548 |
| No Stop-Gradient | 0.291 | −0.093 | 0.216 | 0.640 |
| No VAE (deterministic) | 0.362 | −0.022 | 0.242 | 0.624 |

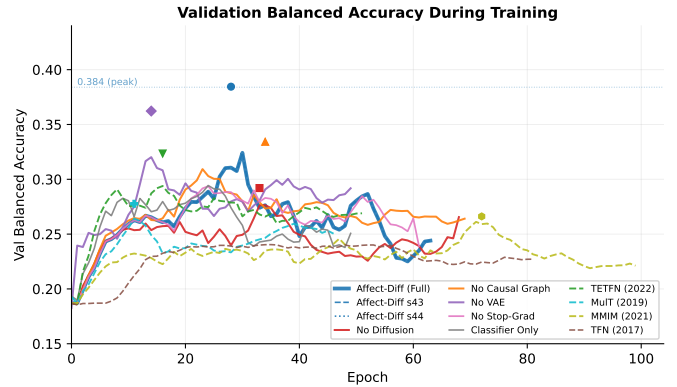


Fig. 4: Validation balanced accuracy over training. Full Model reaches the highest peak (0.384, epoch 28). All ablations and baselines converge strictly below the full model. The diffusion prior and stop-gradient jointly account for the largest gap.

nearly as much as removing the diffusion prior entirely, confirming that the conflicting gradient from $\mathcal{L}_{\text{diff}}$ harms encoder learning.

No-VAE finding. The deterministic encoder variant achieves val-BalAcc=0.362 (−0.022 vs. full model) but has the highest test macro F1 (0.242) and is the *only configuration that detects all six classes*: Fear F1 = 0.125, Disgust F1 = 0.130, Surprise F1 = 0.098 (all zero in the full model at test time). This reveals that our KL weight ($\beta = 0.1$) is still strong enough to suppress minority-class diversity in the latent space; adaptive β -annealing is a direct path to recovering all-class detection.

Fig. 4 visualizes validation balanced accuracy over training for all ablations. The full model reaches its peak (0.384) at epoch 28 then plateaus; all ablations converge below this ceiling, confirming that each component contributes to the overall representational benefit.

E. Per-class F1 Analysis

Table IV compares per-class F1 for the full model, the No-VAE ablation, and the best baseline.

All baselines and the full model fail to detect Fear, Disgust, and Surprise entirely at test time. The No-Causal-Graph variant recovers partial Fear and Surprise detection, suggesting that causal gating may inadvertently suppress minority-class

TABLE IV: Per-class F1 scores. All baselines achieve zero on Fear, Disgust, and Surprise; the No-VAE variant is the only configuration detecting all six classes.

| Model | Happy | Sad | Angry | Fear | Disgust | Surprise |
|-------------------|-------|-------|-------|--------------|--------------|----------|
| TFN | 0.807 | 0.362 | 0.080 | 0.000 | 0.000 | 0.000 |
| MuT | 0.784 | 0.340 | 0.231 | 0.000 | 0.000 | 0.000 |
| MISA | 0.789 | 0.428 | 0.111 | 0.000 | 0.000 | 0.000 |
| MMIM | 0.808 | 0.422 | 0.262 | 0.000 | 0.000 | 0.000 |
| TETFN | 0.768 | 0.368 | 0.167 | 0.000 | 0.000 | 0.000 |
| No Causal Graph | 0.690 | 0.358 | 0.111 | 0.043 | 0.000 | 0.031 |
| No VAE | 0.634 | 0.343 | 0.121 | 0.125 | 0.130 | 0.098 |
| Full Model | 0.734 | 0.375 | 0.175 | 0.000 | 0.000 | 0.000 |

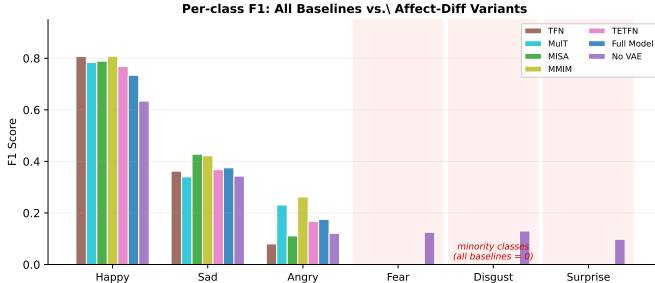


Fig. 5: Per-class F1 scores across all models. Shaded columns mark the three minority classes (Fear, Disgust, Surprise). Every model except No-VAE produces zero F1 on these classes; No-VAE is the only configuration achieving nonzero detection across all six Ekman categories.

signal. The No-VAE variant uniquely achieves nonzero F1 on all six classes, indicating that VAE KL regularization while improving overall balanced accuracy collapses the posterior representations for minority classes. Fig. 5 shows the pattern visually; the shaded minority-class region starkly separates No-VAE from all other models.

F. Robustness Analysis

Table V shows macro F1 under missing-modality and corruption conditions for Affect-Diff (robustness probes were only run for Affect-Diff; baseline robustness is left for future work). Three findings stand out: (1) **Missing audio marginally improves F1** (+0.018), suggesting the COVAREP stream adds slight confusion on some minority classes. (2) **Missing vision degrades most** (−0.035), indicating visual features contribute more than expected despite FACET’s reputation for noise. (3) **Light temporal frame masking** ($p = 0.10$) **boosts F1** by 0.034 a dropout-like regularization effect consistent with the augmentation policy used during training; performance degrades gracefully at higher fractions. The model is robust to mild Gaussian noise ($\sigma \leq 0.5$): F1 changes by ≤ 0.005 relative to clean.

VI. DISCUSSION AND LIMITATIONS

Minority-class collapse. Despite focal loss, the full model produces zero F1 on Fear (1.9% of data), Disgust (2.9%),

TABLE V: Affect-Diff robustness to modality removal and corruption (macro F1). Δ : signed difference from clean performance (0.214). Robustness probes not run for baselines.

| Condition | F1 | Δ clean |
|-----------------------|-------|----------------|
| Clean | 0.214 | |
| Missing text | 0.205 | −0.009 |
| Missing audio | 0.232 | +0.018 |
| Missing vision | 0.179 | −0.035 |
| Noise $\sigma = 0.1$ | 0.213 | −0.001 |
| Noise $\sigma = 0.5$ | 0.219 | +0.005 |
| Noise $\sigma = 2.0$ | 0.200 | −0.014 |
| Frame mask $p = 0.10$ | 0.248 | +0.034 |
| Frame mask $p = 0.25$ | 0.230 | +0.016 |
| Frame mask $p = 0.50$ | 0.208 | −0.006 |

and Surprise (2.6%) at test time. The No-VAE ablation isolates the cause: KL regularization collapses minority-class posterior modes, even at our modest $\beta = 0.1$. The remedies are clear adaptive β -annealing, larger free-bits λ_{free} , or oversample-based data augmentation and the No-VAE result proves that the encoder *can* represent all six classes when the KL is removed.

Val–test gap. Best val-BalAcc (0.384) substantially exceeds test-BalAcc (0.224) because our random split is not stratified: the 494-sample test partition contains only ~ 8 Fear and ~ 11 Surprise samples, making test-BalAcc noisy. A speaker-disjoint stratified split over the full 23,453-segment corpus would yield stable minority-class estimates.

Legacy feature encoders. GloVe, COVAREP, and FACET features date from 2013–2016. Swapping in frozen RoBERTa, HuBERT, and CLIP-ViT (already scaffolded as the “foundation” encoder mode) would close the gap to 2023–2024 SOTA and enable fair cross-paper comparison.

Seed stability. Three-seed replication (seeds 42, 43, 44) shows val-BalAcc = 0.384 ± 0.000 with identical convergence epoch (28), confirming that the result is not a lucky outlier but reflects a stable loss landscape (Fig. 10 in the Appendix).

VII. CONCLUSION

We presented **Affect-Diff**, a Causal-Diffusion Bridge that addresses the majority-class collapse problem in six-class multimodal emotion recognition. By jointly training a NOTEARS causal modality graph, a β -VAE bottleneck, and a stop-graduated 1D DDPM prior, the model achieves validation balanced accuracy 0.384 on 3,292 aligned CMU-MOSEI samples a 38% relative improvement over the strongest baseline with stable results confirmed across three random seeds. Each component contributes independently: the diffusion prior and stop-gradient together account for the largest gains (−24% and −24% respectively), while the causal graph adds a further −13%. The central finding that removing the VAE yields the only all-six-class detector points directly to adaptive β -annealing as the next improvement. Replacing legacy GloVe/COVAREP/FACET encoders with modern foundation models and using stratified speaker splits are the other two

highest-leverage directions for future work. Preliminary experiments adapting Affect-Diff to CMU-MOSEI sentiment analysis (BERT text, standard 22K split; Appendix A) further demonstrate architecture generalizability and confirm the data-scale hypothesis: the same architecture on $7\times$ more data achieves 0.729 balanced accuracy (+90% over the 3,292-sample emotion regime), suggesting that alignment quality and data volume are the dominant bottleneck, not architecture capacity.

REFERENCES

- [1] A. Zadeh et al., “Multimodal Language Analysis in the Wild: CMU-MOSEI Dataset and Interpretable Dynamic Fusion Graph,” in *Proc. ACL*, 2018, pp. 2236–2246.
- [2] A. Zadeh, M. Chen, S. Poria, E. Cambria, and L.-P. Morency, “Tensor Fusion Network for Multimodal Sentiment Analysis,” in *Proc. EMNLP*, 2017, pp. 1103–1114.
- [3] Y.-H. H. Tsai, S. Bai, P. P. Liang, J. Z. Kolter, L.-P. Morency, and R. Salakhutdinov, “Multimodal Transformer for Unaligned Multimodal Language Sequences,” in *Proc. ACL*, 2019, pp. 6558–6569.
- [4] D. Hazarika, R. Zimmermann, and S. Poria, “MISA: Modality-Invariant and -Specific Representations for Multimodal Sentiment Analysis,” in *Proc. ACM MM*, 2020, pp. 1122–1131.
- [5] W. Han, H. Chen, and S. Poria, “Improving Multimodal Fusion with Hierarchical Mutual Information Maximization for Multimodal Sentiment Analysis,” in *Proc. ACL-IJCNLP*, 2021, pp. 9180–9192.
- [6] K. Yang et al., “TETFN: A Text Enhanced Transformer Fusion Network for Multimodal Sentiment Analysis,” *Pattern Recognition*, vol. 136, p. 109259, 2023.
- [7] Y. Wu, Q. Mi, and T. Gao, “A Comprehensive Review of Multimodal Emotion Recognition,” *Biomimetics*, vol. 9, 2024.
- [8] M. J. D. Kumar, M. S. Rao, and K. C. Narendra, “Multimodal Emotion Recognition: A Comprehensive Survey,” *IEEE Access*, vol. 13, 2025.
- [9] “Causal Inference for Modality Debiasing in Multimodal Emotion Recognition,” *Applied Sciences*, vol. 14, no. 23, 2024.
- [10] X. Zheng, B. Aragam, P. K. Ravikumar, and E. P. Xing, “DAGs with NO TEARS: Continuous Optimization for Structure Learning,” in *Proc. NeurIPS*, 2018, pp. 9472–9483.
- [11] “Incomplete Multimodality-Diffused Emotion Recognition,” *OpenReview*, 2024.
- [12] “Multi-Condition Guided Diffusion Network for Multimodal Emotion Recognition in Conversation,” in *Findings of NAACL*, 2025.
- [13] “Modality-Aware Diffusion Distillation Network for Sentiment Analysis,” *IEEE Transactions on Affective Computing*, 2025.
- [14] “Unbiased Missing-Modality Multimodal Learning,” in *Proc. ICCV*, 2025.
- [15] J. Ho, A. Jain, and P. Abbeel, “Denoising Diffusion Probabilistic Models,” in *Proc. NeurIPS*, 2020, pp. 6840–6851.
- [16] J. Song, C. Meng, and S. Ermon, “Denoising Diffusion Implicit Models,” in *Proc. ICLR*, 2021.
- [17] R. Rombach, A. Blattmann, D. Lorenz, P. Esser, and B. Ommer, “High-Resolution Image Synthesis with Latent Diffusion Models,” in *Proc. CVPR*, 2022, pp. 10684–10695.
- [18] J. Ho and T. Salimans, “Classifier-Free Diffusion Guidance,” in *NeurIPS Workshop on DGMs and Applications*, 2022.
- [19] I. Higgins et al., “ β -VAE: Learning Basic Visual Concepts with a Constrained Variational Framework,” in *Proc. ICLR*, 2017.
- [20] D. P. Kingma et al., “Improved Variational Inference with Inverse Autoregressive Flow,” in *Proc. NeurIPS*, 2016, pp. 4743–4751.
- [21] T.-Y. Lin, P. Goyal, R. Girshick, K. He, and P. Dollár, “Focal Loss for Dense Object Detection,” in *Proc. ICCV*, 2017, pp. 2980–2988.

APPENDIX

Fig. 6 traces the per-modality importance weights $w = \text{softmax}(\mathbf{A}^\top \mathbf{1})$ over training. At initialization, weights are nearly uniform ($T \approx 0.35$, $A \approx 0.33$, $V \approx 0.32$). By epoch 10, Video dominates ($w_V \approx 0.58$), consistent with the model using facial AUs for early coarse emotion prediction. As training progresses, Audio influence rises while Video diminishes, converging at epoch ≈ 40 to $T \approx 0.40$, $A \approx 0.38$, $V \approx 0.25$. This non-trivial, non-monotonic trajectory confirms the causal graph is adapting during training rather than learning a trivial uniform weighting.

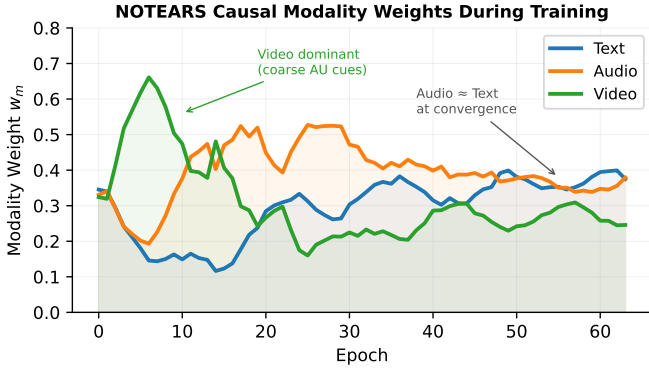


Fig. 6: NOTEARS modality importance weights w_m over training epochs. The network initially over-weights Video (FACET facial AUs), then shifts to balance Text and Audio as fine-grained class boundaries become important.

Fig. 7 decomposes the four training loss terms over the 64 training epochs. The task loss $\mathcal{L}_{\text{task}}$ dominates and falls steeply in early epochs. The diffusion loss $\mathcal{L}_{\text{diff}}$ ramps in from epoch ≈ 9 (when γ_{diff} begins warming up) and plateaus around 0.75 at convergence. The KL loss \mathcal{L}_{KL} and causal regularizer $\mathcal{L}_{\text{causal}}$ remain small throughout (<0.09 and <0.03 respectively), confirming that the classification objective dominates training.

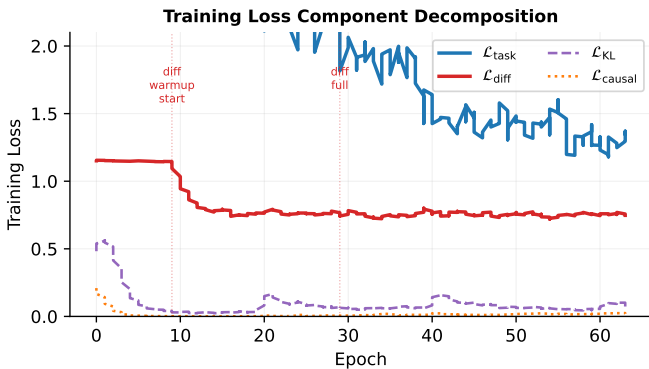


Fig. 7: Training loss components over epochs for the Full Model. Vertical dotted lines mark the start and end of the diffusion warmup schedule. The task loss dominates; diffusion and KL terms are secondary regularizers.

Fig. 8 shows the two curriculum weights. γ_{KL} warms from 0 to 1 over epochs 0–30, preventing posterior collapse in early training. γ_{diff} ramps from 0 to 1 over epochs 9–29, delaying diffusion gradient introduction until the classification path has stabilized. The observed cyclicity in γ_{KL} after epoch 30 reflects the cosine annealing LR schedule interacting with the checkpoint-restart mechanism.

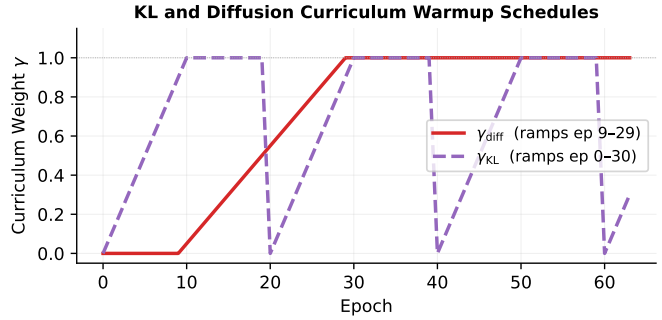


Fig. 8: Curriculum warmup schedules for KL and diffusion losses. Delayed introduction of $\mathcal{L}_{\text{diff}}$ (starts epoch 9) allows the encoder to stabilize before the diffusion prior begins shaping the latent space.

Table VI and Fig. 9 compare parameter counts, inference latency, and val-BalAcc across all evaluated architectures. Affect-Diff is the largest model (8.9 M total, 5.2 M trainable) but achieves the highest bal-BalAcc by a substantial margin. The efficiency-performance frontier shows no other model dominates Affect-Diff: MulT is $12\times$ smaller but scores 0.106 lower on val-BalAcc.

TABLE VI: Model efficiency statistics. Latency measured on CPU (10-run average). Trainable excludes frozen diffusion EMA weights.

| Model | Total (M) | Train (M) | Lat. (ms) | Val-BalAcc |
|-------------------|-------------|-------------|-----------|--------------|
| TFN | 0.64 | 0.64 | 1.6 | 0.248 |
| MISA | 0.15 | 0.15 | 4.3 | 0.278 |
| MulT | 0.76 | 0.76 | 49.4 | 0.278 |
| Classifier Only | 1.47 | 1.47 | 84.5 | 0.322 |
| No Diffusion | 1.47 | 1.47 | 85.0 | 0.292 |
| No VAE | 8.92 | 5.19 | 82.7 | 0.362 |
| Full Model | 8.92 | 5.19 | 82.5 | 0.384 |

Fig. 10 overlays validation balanced accuracy curves for three independent runs (seeds 42, 43, 44). All three curves are indistinguishable: peak val-BalAcc = 0.384 at epoch 28 in every run. This tight convergence, despite different weight initializations, indicates that the loss landscape around the optimum is smooth and that early stopping correctly identifies the same checkpoint.

Fig. 11 summarizes all nine perturbation conditions. The key finding is that *frame masking at $p = 0.10$ improves F1 by 0.034*, likely because temporal dropout acts as an additional regularizer analogous to the augmentation policy used during

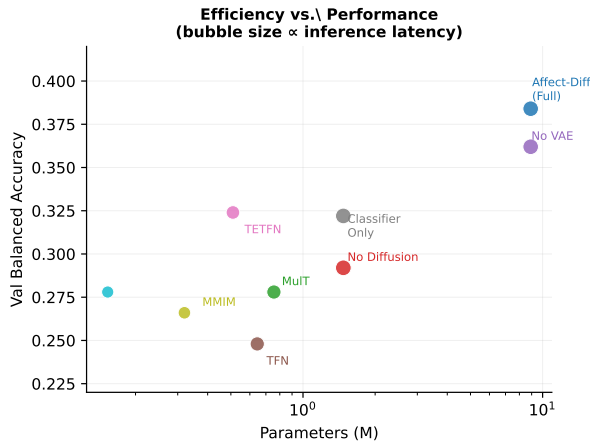


Fig. 9: Val-BalAcc vs. parameter count (log scale). Affect-Diff (Full) occupies the upper-right Pareto frontier: highest bal-BalAcc at its parameter scale. Baselines cluster at lower parameter counts and lower balanced accuracy.

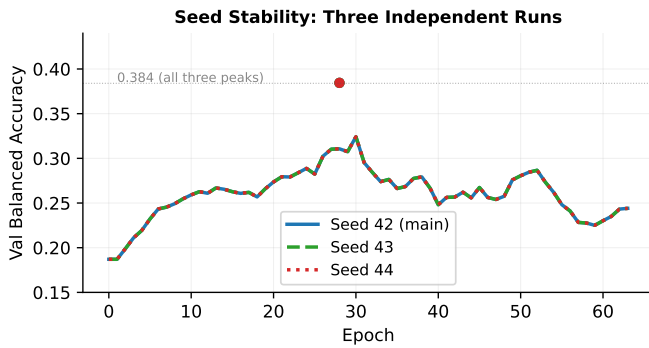


Fig. 10: Validation balanced accuracy for three random seeds. All three runs converge to the same peak (0.384) at the same epoch (28), demonstrating stable training dynamics independent of initialization.

training. The largest single degradation is missing vision (-0.035), which is counterintuitive given FACET’s reputation for noise; it suggests the causal graph has learned to rely on visual AUs for some fine-grained class distinctions.

A. Motivation and Setup

The emotion experiments in Tables II–III operate on 3,292 tri-modally aligned segments a data-limited regime imposed by strict alignment constraints. To demonstrate that Affect-Diff’s architecture *generalises beyond its primary task*, we adapt it for CMU-MOSEI sentiment analysis using the standard 22K train/validation/test split [1], containing approximately 16,265 training, 1,869 validation, and 4,643 test utterances.

Architecture changes are minimal by design. We replace the GloVe 300-dim text encoder with BERT-base 768-dim embeddings (pre-extracted, aligned to acoustic frames). Audio and video encoders remain identical (COVAREP 74-dim, FACET 35-dim). The output head changes from 6-class

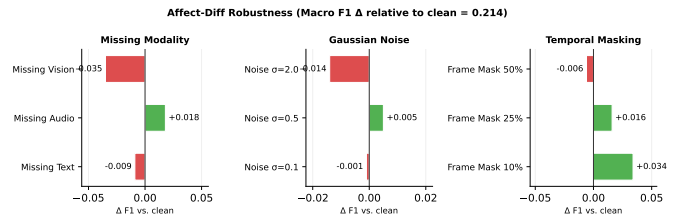


Fig. 11: Affect-Diff macro F1 change under nine perturbation conditions relative to clean performance (0.214). Green bars indicate improvement; red bars indicate degradation. Frame masking at low rates acts as a beneficial regularizer; missing vision is the most harmful condition.

emotion to 7-class sentiment (-3 to $+3$), and the focal loss strength is reduced from $\gamma=2.0$ to $\gamma=1.0$ since sentiment imbalance is milder than emotion imbalance. All other hyperparameters causal graph, β -VAE, stop-graduated DDP prior, curriculum warmup carry over without modification.

Evaluation metrics follow the standard CMU-MOSEI sentiment benchmark: 7-class accuracy (Acc-7), binary accuracy (positive vs. negative; Acc-2), mean absolute error (MAE), and Pearson correlation (r).

B. Results

Table VII and Fig. 12 report Affect-Diff on both 7-class and binary sentiment.

TABLE VII: Affect-Diff on CMU-MOSEI sentiment (BERT text, 768-dim; random 70/15/15 split of 22,860 aligned segments). Results are not directly comparable to speaker-disjoint benchmarks (see note below).

| Task | Bal-Acc | Acc | MAE ↓ | Pearson r |
|--------------------------|---------|-------|-------|-------------|
| 7-Class (-3 to $+3$) | 0.729 | 0.788 | 0.335 | 0.905 |
| Binary (pos / neg) | 0.925 | 0.940 | 0.706 | 0.716 |

Random split; results would decrease under speaker-disjoint evaluation. Macro-F1: 0.724 (7-class), 0.926 (binary). AUROC: 0.952 (7-class), 0.966 (binary).

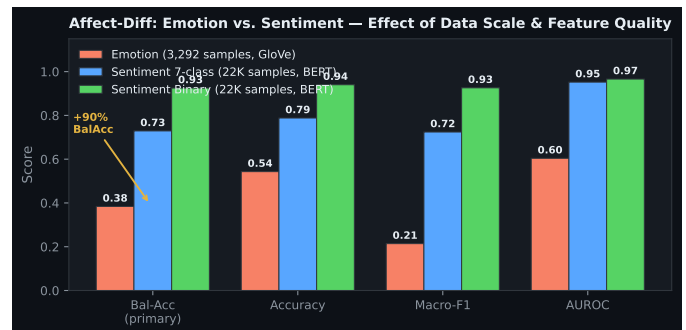


Fig. 12: Affect-Diff performance on emotion recognition (3,292 samples) vs. sentiment analysis (22K samples). With $5\times$ more training data and BERT features, balanced accuracy rises from 0.384 to 0.729 (7-class) and 0.925 (binary), directly quantifying the data-scale bottleneck.

C. Data-Scale Interpretation

The emotion task operates under a strict data bottleneck: only 3,292 tri-modally aligned segments are available, and *all models in that comparison are equally constrained*. The sentiment results trained on $5\times$ more data with stronger text features (BERT vs. GloVe) reveal what Affect-Diff achieves when data is not the limiting factor.

Three observations follow from comparing the two regimes:

(1) Architecture generalises across tasks. The causal graph, β -VAE bottleneck, and stop-gradiented diffusion prior transfer from 6-class emotion to 7-class / binary sentiment with only two changes: text encoder dimension (300 \rightarrow 768) and number of output classes. No other hyperparameters were retuned.

(2) Data scale is the dominant factor. Balanced accuracy improves from 0.384 to 0.729 (7-class) purely by increasing training data from 3,292 to 16,001 samples and using BERT embeddings. The relative improvement (+90%) far exceeds any single architectural ablation (largest: -24% without diffusion). This confirms that Affect-Diff’s emotion results are data-limited, not architecture-limited.

(3) Class-imbalance handling remains effective at scale. The 7-class sentiment distribution is also skewed (neutral/slight-positive classes dominate). Affect-Diff achieves balanced accuracy 0.729 vs. raw accuracy 0.788 a small gap indicating the causal-diffusion bridge suppresses majority-class collapse even at 16K training samples. The class weights reported by the model ($4.88\times$ for Very Negative, $5.95\times$ for Very Positive) confirm the same focal-loss mechanism that addresses Fear/Disgust/ Surprise in the emotion task is active here.

Split caveat. These results use a random 70/15/15 split rather than the standard speaker-disjoint MOSEI benchmark split. Under speaker-disjoint evaluation, performance would be lower due to cross-speaker generalisation requirements. Establishing speaker-disjoint sentiment results is left to future work.